



Construction of ratiometric hydrogen sulfide probe with two reaction sites and its applications in solution and in live cells

Deyang Fu^a, Weiru Zhi^a, Lihua Lv^a, Yi Luo^b, Xiaoqing Xiong^{a,b,*}, Xiaohui Kang^{b,c,**}, Wei Hou^a, Jun Yan^a, Hongjuan Zhao^a, Laijiu Zheng^a

^a Key Lab of Textile Cleaning, Dalian Polytechnic University, #1 Qinggongyuan, Dalian 116034, PR China

^b State Key Laboratory of Fine Chemicals, Dalian University of Technology, #2 Linggong Road, Dalian 116024, PR China

^c College of Pharmacy, Dalian Medical University, Western 9 Lvshun nan Road, Dalian 116044, PR China

ARTICLE INFO

Article history:

Received 2 April 2019

Received in revised form 28 June 2019

Accepted 14 July 2019

Available online 17 July 2019

Keywords:

Hydrogen sulfide probe

Ratiometric fluorescence changes

Two reaction sites

Fluorescence imaging

ABSTRACT

Hydrogen sulfide (H₂S), as the third multifunctional signaling biomolecule, it acts as a neuromodulator in the human brain and is recognized as an important gas transmitter in human physiology. The abnormal concentrations of H₂S in human cells can result in several common diseases. Therefore, accurate, fast, and reliable methodologies are required for measuring the in vitro and in vivo concentrations of H₂S to further investigate its function. In this study, a novel **DR-SO₂N₃** fluorescent probe containing the fluorophore **Disperse Red 277** and a sulfonyl azide group was developed and exploited based on the structural characteristic of **Disperse Red 277** that contains the active site easily can be attacked by HS⁻. Therefore, this probe featured two reaction sites that involved the reduction and Michael addition of H₂S and exhibited rapid ratiometric fluorescence changes and high selectivity towards H₂S with a 619-fold enhancement factor. Further, the density functional theory (DFT)/time-dependent density functional theory (TDDFT) studies are conducted to understand the photophysical properties of **DR-SO₂N₃** and the final product **DRHS-SO₂NH₂**, which makes the proposed mechanism more reasonable. Furthermore, the probe was successfully applied for the ratiometric fluorescence imaging of exogenous H₂S in living cells.

© 2019 Elsevier B.V. All rights reserved.

1. Introduction

H₂S is a renowned, colorless, highly toxic, and acid gas with an unpleasant rotten egg odor [1–3]. H₂S can affect the eyes as well as the respiratory and central nervous systems even in low exogenous concentrations. Endogenous H₂S is produced using L-cysteine in the reactions that are catalyzed by cystathionine-synthase (CBS) or cystathionine-lyase (CSE) [4] and transformed [5]. Therefore, H₂S is considered to be the third multifunctional signaling biomolecule along with NO and CO [6] because it acts as a neuromodulator in the human brain and is recognized as an important gas transmitter in human physiology [7]. Currently, scientists have observed that the production of abnormal concentrations of H₂S in human cells can result in several common diseases [1,8], including Alzheimer's disease [9], Down's syndrome [10], and liver cirrhosis [11], which explains the increasing

amount of attention that is being devoted to H₂S detection and determination in living systems. Currently, various methods, including both chemical methods (iodometric, mercury, methylene blue colorimetric, and lead acetate reaction rate) and physical methods (chromatography, laser, and H₂S sensor), are available for detecting H₂S [12–14]; however, all the aforementioned methods are complicated and time-consuming. Therefore, accurate, fast, and reliable methodologies are still required for measuring the in vitro and in vivo concentrations of H₂S to further investigate its function.

Recently, some fluorescent detection methods have been observed to be particularly powerful because of their high sensitivities, specificities, and minimal toxicities in cells and tissues [15–21]. Accordingly, various fluorescent probes have been developed for the detection of H₂S based on different chemical reactions of H₂S, including its reduction property, high binding affinity towards Cu²⁺ ions [22], azide reduction [12,23–33], specific nucleophilicity [34–36], and thiolysis of dinitrophenyl ether [6,37]. Among these strategies, the introduction of an azide or sulfonyl azide group into fluorescent dyes for its reduction by H₂S has been commonly applied. For example, Peng's group used the "TURN-ON" fluorescence of the H₂S probe **1-NH₂** through the reduction of azide by H₂S [38]. However, the "TURN-ON" fluorescence

* Correspondence to: X. Xiong, Key Lab of Textile Cleaning, Dalian Polytechnic University, #1 Qinggongyuan, Dalian 116034, PR China.

** Correspondence to: X. Kang, College of Pharmacy, Dalian Medical University, Western 9 Lvshun nan Road, Dalian 116044, PR China.

E-mail addresses: xiongxq@dipu.edu.cn (X. Xiong), kangxh@dmu.edu.cn (X. Kang).

may be influenced because of environmental factors in real applications. To avoid this negative interference, it is highly desirable to develop fast response probes for H_2S based on accurate ratiometric fluorescent probes that can self-calibrate using two emission intensities [30,39–41]. In addition, many reported H_2S probes always simultaneously detected biothiols [1,42] such as cysteine (Cys), homocysteine (Hcy), and glutathione (GSH), viscosity [43], HClO [23], NO [25] and so on, thus, these probes showed low selectivity towards H_2S . Even some probes could discriminate H_2S and the other species, the detection process was very complicated through different emission channels. Thus, H_2S fluorescent probes with simple detection process and high selectivity should be proposed.

Various characteristics, such as high quantum yield, long-wavelength emission, and response to H_2S by fluorescent changes, should be considered while selecting a fluorophore. Coumarin and its derivatives always own the aforementioned properties, thus, they are commonly and extensively used in several applications, including cell biology [44], lasers [45], sensors [46], and advanced photophysical systems. In particular, iminocoumarin (**Disperse Red 277**) is an important coumarin dye whose derived fluorophores are renowned for their bright fluorescent emissions and highly efficient quantum yields [47], which are suitable for various biological applications. However, when compared to coumarin, the usage of **Disperse Red 277** in fluorescent probes is still scarce and is limited to one report describing that the iminocoumarin moiety can be incorporated as the fluorescent signaling unit in the Zn^{2+} indicator [48]. To the best of our knowledge, **Disperse Red 277** and its derivatives have not been used so far for the development of fluorescent probes that are capable of detecting and imaging H_2S , which would be highly valuable but even more challenging. As matter of fact, the structure of **Disperse Red 277** may provide the possibility to detect H_2S because the HS^- group can take place nucleophilic addition to an electron-poor α,β -unsaturated $\text{C}=\text{C}$ double bond (site II, Scheme 1).

By considering the aforementioned requirements and theoretical facts, in this study, we describe the realization of an effective ratiometric fluorescent probe (**DR-SO₂N₃**) for H_2S based on the derivatization of **Disperse Red 277**, which could discriminate H_2S from other biothiols

using the reduction and Michael addition of HS^- . It is worth noting that the new **DR-SO₂N₃** probe exhibits physical properties that are similar to those of **Disperse Red 277**. Furthermore, we have utilized the DFT/TDDFT calculation for rationalizing the optical properties of **DR-SO₂N₃** and final product between **DR-SO₂N₃** and H_2S . Additionally, the sensing properties of **DR-SO₂N₃** were investigated to denote that this probe exhibited rapid ratiometric fluorescence changes and high H_2S selectivity. Bioimaging studies have demonstrated that the **DR-SO₂N₃** probe exhibited good permeability, low cytotoxicity, and ratiometrically detected endogenous H_2S in living cells. These data provide us with a new platform to study the function of H_2S in biological systems.

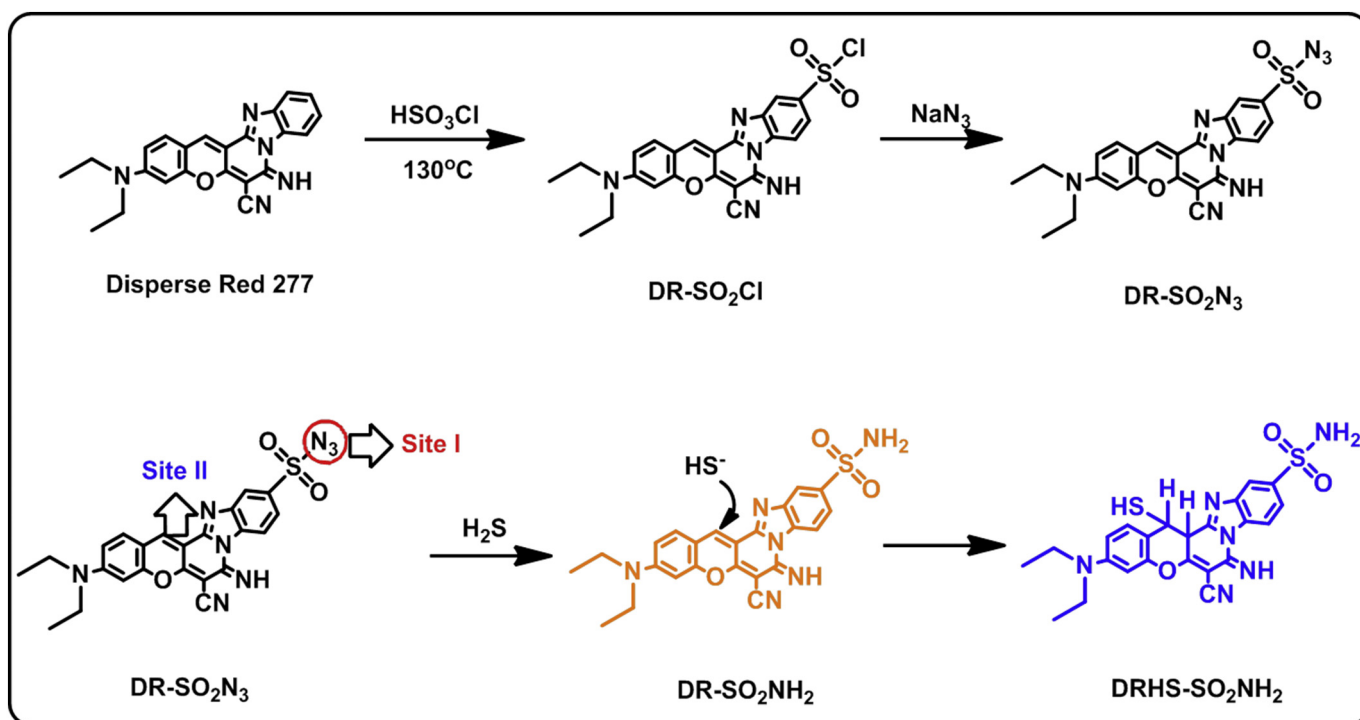
2. Experimental section

2.1. Materials

The common reagents used in the experiments were all of analytical grade. 4-N,N-diamino-2-hydroxybenzaldehyde, 2-cyanogen methyl benzimidazole, 3-(2-benzimidazole)-7-diamine coumarin, malononitrile, chlorosulfonic acid, and sodium azide were purchased from Aladdin. Rhodamine B was purchased from Tianjin Fine Chemicals Development Center. ^1H NMR and ^{13}C NMR spectra were recorded on a VARIAN INOVA-400 spectrometer with chemical shifts being reported as ppm (in DMSO, TMS as internal standard). The following abbreviations are used to indicate the multiplicities: s, singlet; d, doublet; t, triplet; q, quartet; m, multiple; and br, broad. The mass spectrometric data were obtained on a Q-TOF Micro mass spectrometer. Further, the UV-vis spectra were collected on a Perkin Elmer Lambda 35 UV-vis spectrophotometer. The fluorescence measurements were performed using a VAEIAN CARY Eclipse Fluorescence Spectrophotometer (Serial No. FL1109-M018), and the fluorescence images of the MCF-7 cells were obtained using an Olympus FV1000 laser confocal microscope.

2.2. Synthesis of DR-SO₂N₃

4-N,N-Diamino-2-hydroxybenzaldehyde (2.0 g, 0.01 mol) and 2-cyanogen methyl benzimidazole (1.67 g, 0.01 mol) were dissolved in



Scheme 1. Design and synthetic routine of **DR-SO₂N₃** and the rationale of the designing mechanism

ethanol (0.07 g, 0.001 mol), and pyridine was added as the catalyst into the reaction system at room temperature (25 °C). The mixture was stirred for 24 h, and the product was filtered, washed with ethanol, and dried. 3-(2-Benzimidazole)-7-diamine coumarin (2.0 g, 0.006 mol), malononitrile (0.6 g, 0.009 mol), and ethylene glycol monomethyl ether (20 mL) were further added. The mixture was refluxed for 5 h to obtain **Disperse Red 277** (1.9 g, 0.004 mol, yield 82%), which was used in the subsequent step without any purification. In the ice water bath, chlorosulfonic acid (30 mL) was added to **Disperse Red 277** (2.0 g, 0.005 mol), and the mixture was refluxed at 130 °C for 3.5 h. After the mixture was cooled to room temperature and poured into ice water, an orange-red solid was precipitated. The precipitate was washed using cold water until the pH was adjusted to approximately 5. The **DR-SO₂Cl** compound was obtained after being dried and grinded. Next, sodium azide (0.124 g, 0.002 mol) dissolved in water/ethanol (3 mL:3 mL) was added to a solution of **DR-SO₂Cl** (0.5 g, 0.001 mol) in ethanol (50 mL), and the mixture was stirred at 80 °C for 24 h. Further, the solvents were evaporated under vacuum, and **DR-SO₂N₃** (0.38 g, 0.0008 mol, yield 80%) was obtained as a dark red solid powder ($R_f = 0.35$; 5% CH₃OH in dichloromethane). ¹H NMR (400 MHz, DMSO *d*₆) δ 9.32 (s, 1H), 8.85 (d, *J* = 8.3 Hz, 1H), 8.04 (d, *J* = 2.9 Hz, 2H), 7.82 (d, *J* = 9.0 Hz, 1H), 7.08–6.96 (m, 1H), 6.84 (s, 1H), 5.77 (s, 1H), 3.61 (q, *J* = 6.8 Hz, 4H), 1.21 (t, *J* = 6.9 Hz, 6H). ¹³C NMR (100 MHz, DMSO *d*₆) δ 161.53, 155.96, 154.42, 152.67, 149.76, 148.93, 137.61, 133.04, 131.50, 131.15, 123.84, 120.20, 117.06, 114.73, 112.67, 110.68, 105.45, 97.08, 49.06, 45.29, 12.90. MS (API ESI⁺): *m/z*: calcd for C₂₃H₁₈N₈O₃S: 486.12; found 487.1301 M + 1.

2.3. Spectroscopic and fluorescence quantum yield measurements

The relative fluorescence quantum yields were determined with Rhodamine B as the standard and calculated using the following equation [49,50]:

$$\Phi_x = \Phi_s (F_x/F_s)(A_s/A_x)(\lambda_{\text{exs}}/\lambda_{\text{exx}})(n_x/n_s)^2,$$

where Φ_x represents the quantum yield, *F* denotes the integrated area under the corrected emission spectrum, *A* denotes the absorbance at the excitation wavelength, λ_{ex} denotes the excitation wavelength, *n* denotes the refractive index of the solution (because of the low concentrations of the solutions (10⁻⁷–10⁻⁸ M), the refractive indices of the solutions were replaced with those of the solvents); and the subscripts *x* and *s* refer to the unknown and the standard, respectively.

2.4. Cell incubation and fluorescence imaging

The MCF-7 cells were obtained from the State Key Laboratory of Fine Chemicals in the Dalian University of Technology. The cells were seeded onto cover slips at a concentration of 2 × 10⁴ cells mL⁻¹ and cultured in Dulbecco's modified eagle medium (DMEM) in an incubator (37 °C, 5% CO₂, and 20% O₂). After 24 h, the cover slips were slightly rinsed thrice using phosphate buffer saline (PBS) to remove the media and then cultured in DMEM for later use. First, the **DR-SO₂N₃** (10 μM) and **Disperse Red 277** (10 μM) dyes were added to the aforementioned cellular samples and incubated for 30 min; next, the samples were slightly rinsed thrice using PBS and observed using an Olympus FV1000 confocal fluorescence microscope to obtain pictures with white light and fluorescence with the help of a confocal fluorescence image captured using 100× objective lens. Then, the cells were treated using fresh medium containing Na₂S (150.0 μM) for an additional 15 min, and the corresponding luminescence images were observed using the same imaging method.

3. Results and discussion

3.1. Molecular design and synthesis of DR-SO₂N₃

The design of the **DR-SO₂N₃** probe utilizing the coumarin dye **Disperse Red 277** is depicted in Scheme 1. The probe has two potential reaction sites as fluorophores: a renowned fluorescence quencher sulfonyl azide group that lies in the benzimidazole moiety as the reaction site for H₂S (site I) and an α,β-unsaturated bond in the coumarin moiety as the Michael acceptor (site II). This structural feature was expected to contribute to the activity of the probe. We assumed that the **DR-SO₂N₃** probe could discriminate between H₂S and other biothiols and the biologically related species with high accuracy based on the reduction and nucleophilicity of HS⁻. Further, the reaction between **DR-SO₂N₃** and H₂S would provide **DR-SO₂NH₂** as an intermediate because of the rapid reduction of HS⁻ at site I. Subsequently, the Michael adduct **DRHS-SO₂NH₂** would be produced by intramolecular nucleophilic attack of HS⁻ at site II. These hypotheses are partially supported by the recent publications that have investigated the intermediate and final product of the reaction.²⁵ The selective discrimination of H₂S would be feasible because of the weak reduction potential and nucleophilicity of the remaining biothiols. Furthermore, the ratiometric monitoring of cellular H₂S could be accomplished, which will be useful for clarifying the role of H₂S in physiological processes. The structure of **DR-SO₂N₃** was elucidated using ¹H and ¹³C nuclear magnetic resonance (NMR) spectroscopy and high-resolution mass spectrometry analyses (see supporting information).

3.2. Photophysical properties and the DFT/TDDFT studies of DR-SO₂N₃

The photophysical properties of the **DR-SO₂N₃** probe were initially investigated using different solvents and were compared with those of **Disperse Red 277** (Tables S1 and S2). Further, the maximum absorption and emission wavelengths of **DR-SO₂N₃** were observed to be similar to those of **Disperse Red 277**. In dimethyl sulfoxide (DMSO), the UV-vis spectrum of **DR-SO₂N₃** exhibited two main absorption peaks at 362 and 553 nm and two emission peaks at 460 and 583 nm. The fluorescence quantum yield of **DR-SO₂N₃** ($\Phi_{\text{DR-SO}_2\text{N}_3}$) was established to be 0.45 in DMSO (Table S1). The $\Phi_{\text{DR-SO}_2\text{N}_3}$ value was slightly lower than that of **Disperse Red 277** (Table S2), which indicated that the introduction of the sulfonyl azide group did not completely quench the fluorescence of **DR-SO₂N₃**.

To rationalize the optical properties of the new functional dye **DR-SO₂N₃**, frontier molecular orbital analysis was conducted based on the DFT/TDDFT calculation at the B3LYP/6-311 + G** level with Gaussian 09 in comparison with **Disperse Red 277** (Fig. 1), considering the solvation effect of DMSO using the solvent model density (SMD). The results confirmed that the two strongest absorption bands that were experimentally observed for **Disperse Red 277** were obtained from the excited states S₁ and S₅ and corresponded to two main electronic transitions (highest occupied molecular orbital (HOMO) → lowest occupied molecular orbital (LUMO), $f_{\text{ab}} = 1.079$ and $\lambda_{\text{ab}} = 492$ nm; HOMO-3 → LUMO, $f_{\text{ab}} = 0.169$, and $\lambda_{\text{ab}} = 332$ nm), respectively (Table S3). The observation of the frontier molecular orbitals analysis reveals that HOMO and LUMO are mainly located on the coumarin moiety, whereas HOMO-3 is mainly located on the benzimidazole moiety. Therefore, the two remarkable absorption bands of **Disperse Red 277** can be ascribed to the $\pi \rightarrow \pi^*$ transitions from the coumarin and benzimidazole moieties to the coumarin moiety. Further, the calculated emission spectroscopic data denoted that the S₁ → S₀ (LUMO → HOMO, $f_{\text{em}} = 1.296$, and $\lambda_{\text{em}} = 573$ nm) and S₅ → S₀ (LUMO → HOMO-3, $f_{\text{em}} = 0.349$, and $\lambda_{\text{em}} = 350$ nm) transitions corresponded to two emission peaks at 584 and 463 nm, respectively (Table S4); this observation was in good agreement with the experimental results. Further, when the benzene ring of the benzimidazole moiety in **Disperse Red 277** was modified using the sulfonyl azide group for generating **DR-SO₂N₃**, two main

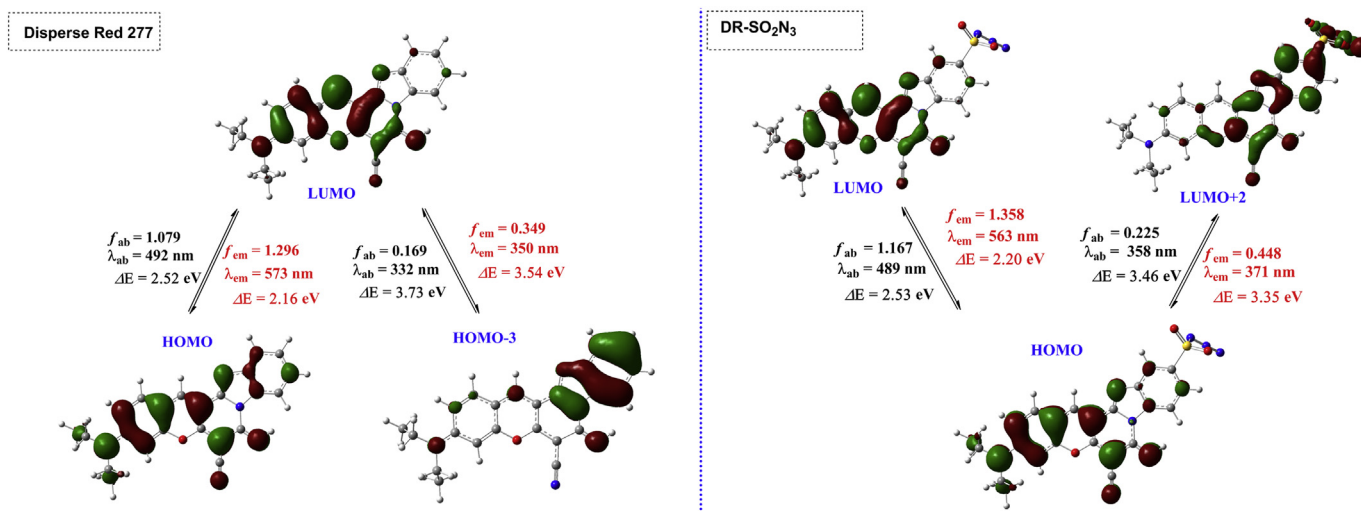


Fig. 1. The frontier molecular orbital plots of **Disperse Red 277** and **DR-SO₂N₃** in DMSO; they are involved in vertical excitation (UV-vis absorption) and emission.

absorption bands were observed for **DR-SO₂N₃**, which were attributed to the HOMO→LUMO ($f_{ab} = 1.167$ and $\lambda_{ab} = 489$ nm) and HOMO→LUMO+2 ($f_{ab} = 0.225$ and $\lambda_{ab} = 358$ nm) transitions (Table S5). The electron transfers from the coumarin moiety resulted in a short wavelength absorption band at 358 nm because LUMO+2 was mainly located on the benzimidazole and sulfonyl azide moieties. Meanwhile, the calculated emission data of **DR-SO₂N₃** were similar to that of **Disperse Red 277**. Thus, the emission transitions were attributed to $S_1 \rightarrow S_0$ (LUMO→HOMO, $f_{em} = 1.358$, and $\lambda_{em} = 563$ nm) and $S_4 \rightarrow S_0$ (LUMO+2 → HOMO, $f_{em} = 0.448$, and $\lambda_{em} = 371$ nm) (Table S6). Even though the optical results for both **Disperse Red 277** and **DR-SO₂N₃** that are obtained from the frontier molecular orbital analysis did not completely agree with the experimental results, these results shed some light on the luminescence mechanism of **DR-SO₂N₃**. Regardless, it can be concluded that the high fluorescence quantum yield of this system may be useful for detecting H₂S.

3.3. Sensing properties of DR-SO₂N₃ to H₂S

To understand the sensing behavior of the **DR-SO₂N₃** probe towards H₂S, it was subjected to the absorbance and fluorescence titration

experiments. Further, the absorbance and fluorescence intensity changes of the **DR-SO₂N₃** probe were recorded upon the addition of Na₂S because Na₂S is commonly used as the source of H₂S. Upon the addition of 1 equiv. Na₂S, a slight increase could be observed in the fluorescence intensity of the bands at 435 and 584 nm. This is most likely because of the reaction of the fluorescence quencher sulfonyl azide with H₂S producing the intermediate **DR-SO₂NH₂** by the reduction of azide to amine. Further, the mixture was treated using the gradient concentrations of Na₂S (from 3 to 150 equiv.), and a remarkable decrease in the fluorescence intensity of the peak could be observed at 584 nm, whereas the emission peak gradually increased at 435 nm (Fig. 2). The enhanced emission at 435 nm may be associated with the formation of the final product **DRHS-SO₂NH₂**. These changes in fluorescence intensity after the occurrence of the reaction imply that the **DR-SO₂N₃** probe can ratiometrically respond to the target H₂S. The ratiometric response of the fluorescence intensities at 435 and 584 nm ($F_{435\text{ nm}}/F_{584\text{ nm}}$) increased from 0.16 to 98.98 before and after the reaction, with a final 619-fold enhancement factor. As depicted in Fig. S1, the fluorescence signal ratio $F_{584\text{ nm}}/F_{435\text{ nm}}$ was linearly related with the concentration of Na₂S ranging from 0 to 28 μM . Under well-established sensing conditions, the limit of detection was calculated to be 2.46 μM

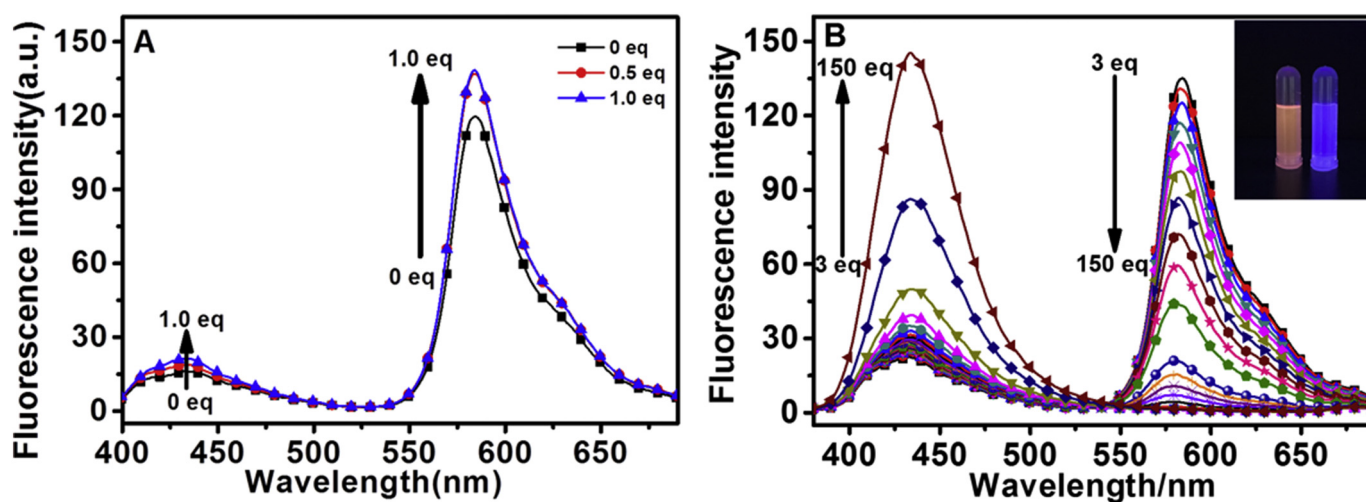


Fig. 2. (A) Fluorescence spectral changes of **DR-SO₂N₃** (5.0 μM in the DMSO/HEPES buffer = 6/4) after incubation with different Na₂S concentrations (0, 0.5, and 1.0 equiv.). (B) Fluorescence spectral changes of **DR-SO₂N₃** (5.0 μM in DMSO/HEPES buffer = 6/4) after incubation with different concentrations of Na₂S (3.0 → 150 equiv.). Each spectrum was recorded after 60 s. The inset denotes the color change of **DR-SO₂N₃** (5.0 μM) in the absence of Na₂S (left) and the presence of 150 equiv. Na₂S (right).

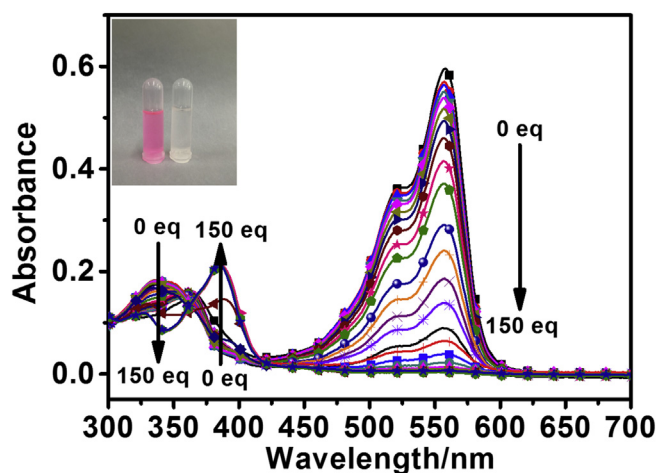


Fig. 3. Absorption spectral changes of **DR-SO₂N₃** (5.0 μ M in DMSO/HEPES buffer = 6/4) after incubation with different concentrations of **Na₂S** (0 \rightarrow 150 equiv.). Each spectrum was recorded after 60 s. The inset denotes the color change of **DR-SO₂N₃** (5.0 μ M) in the absence of **Na₂S** (left) and the presence of 150 equiv. **Na₂S** (right).

according to the definition by $3\sigma/k$ (where σ is the standard deviation of the blank sample and k is the slope of the linear regression equation).

Further, the results of the absorption experiments are presented in Fig. 3. As can be observed, the initial absorption peak of **DR-SO₂N₃** at 366 nm decreased and exhibited a 36-nm blue shift to 330 nm after the addition of **Na₂S**. Furthermore, a new peak could be observed at 386 nm with a distinct isosbestic point at 355 nm, whereas the absorption peak at 555 nm exhibited a drastic decrease, which was accompanied by an apparent change in color from pink to almost colorless (inset of Fig. 3). The absorption peak at 330 nm may be assigned to the **DR-SO₂NH₂** intermediate, whereas the absorption peak at 355 nm may be attributed to the final product **DRHS-SO₂NH₂**. This indicates that the conjugation between coumarin and benzimidazole sulfonyl azide was broken because of the Michael addition of HS^- to site II in the probe, which allowed for the colorimetric detection of H_2S by the naked eye. Based on these results, it can be concluded that changes in absorption and emission are likely to be associated with the formation of the final product **DRHS-SO₂NH₂**.

By considering the relevance of the response time for fluorescence probes, the time-dependent fluorescence intensities at 584 and 435 nm at varied concentrations of HS^- were monitored. As can be observed from Fig. 4, the fluorescence intensity at 584 nm exhibited a

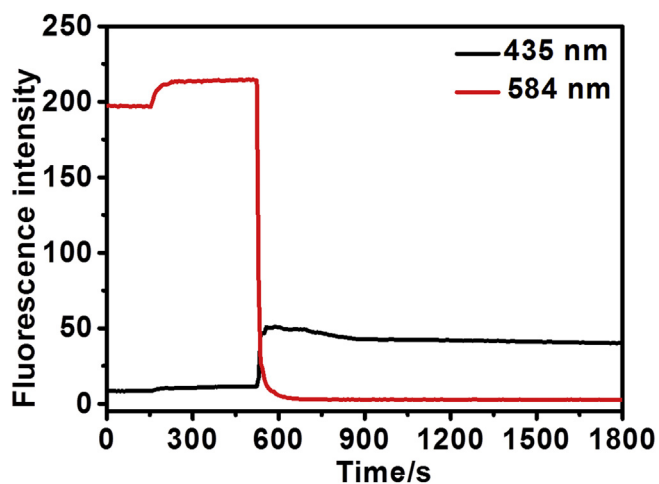


Fig. 4. Time course of the fluorescence response ($\lambda_{\text{em}} = 435$ and 584 nm) of the **DR-SO₂N₃** probe (5.0 μ M) in an aqueous solution (5.0 μ M in DMSO/HEPES buffer = 6/4) with respect to the presence of 1 and 150 equiv. **Na₂S** and an excitation at 340 nm.

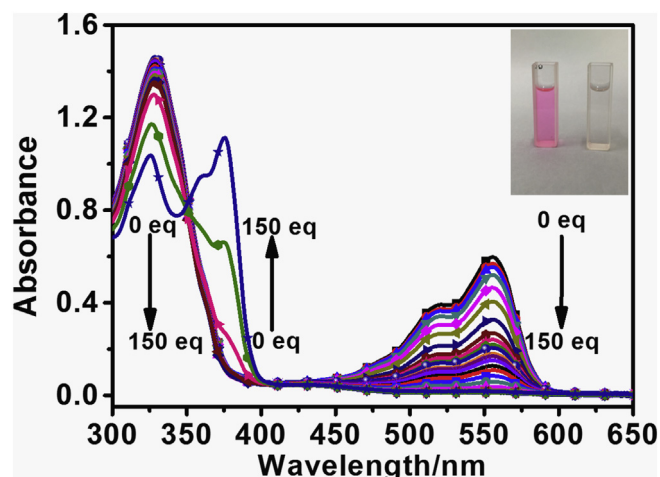


Fig. 5. Absorption spectral changes of **Disperse Red 277** (5.0 μ M in DMSO/HEPES buffer = 6/4) after incubation with different concentrations of **Na₂S** (0 \rightarrow 150 equiv.). Each spectrum was recorded after 60 s. The inset denotes the color change of **Disperse Red 277** (5.0 μ M) in the absence of **Na₂S** (left) and the presence of 150 equiv. **Na₂S** (right).

slight enhancement when the concentration of **Na₂S** became 1 equiv., whereas the peak at 435 nm remained virtually unaltered. Conversely, the latter fluorescence intensity at 435 nm increased after the addition of more than 3 equiv. **Na₂S**, whereas that at 584 nm decreased, which was consistent with the results of the **Na₂S** titration experiments. All the changes with respect to the fluorescence intensities were observed to occur within 60 s, indicating the rapid response ability of the **DR-SO₂N₃** probe to H_2S .

To investigate the selectivity of **DR-SO₂N₃**, which is another key factor for a probe, it was treated with various relevant interference species (such as representative amino acids, metal ions, and anions) and monitored by emission spectroscopy. The results denoted that no noticeable changes were observed in the fluorescence histogram upon the addition of biothiols (Cys, Hcy, and GSH), metal ions (K^+ , Cu^{2+} , Al^{3+} , Ca^{2+} , and NH_4^+), and anions (Br^- , NO_3^- , I^- , PO_4^{3-} , HSO_3^- , SCN^- , and SO_3^{2-}), aminos (glycine, alanine, and valine), reactive oxygen species (H_2O_2 , ClO^-), and reactive nitrogen species (NO_2^-), which confirmed that the **DR-SO₂N₃** probe could distinguish H_2S from other biothiols and relevant interference (Fig. S2). The excellent performance of the **DR-SO₂N₃** probe renders it applicable for sensing intracellular H_2S .

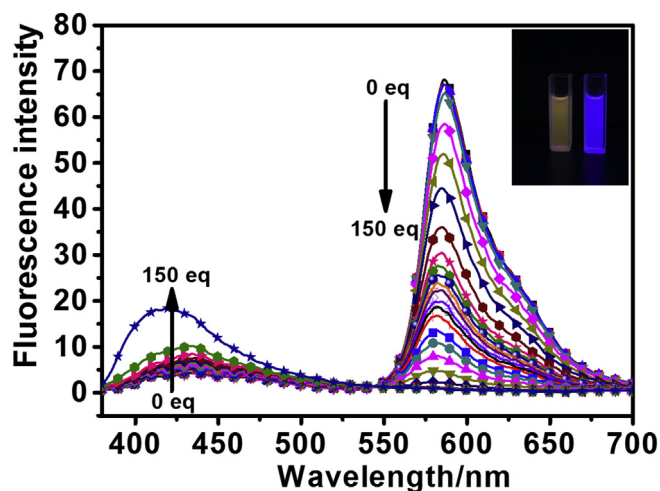
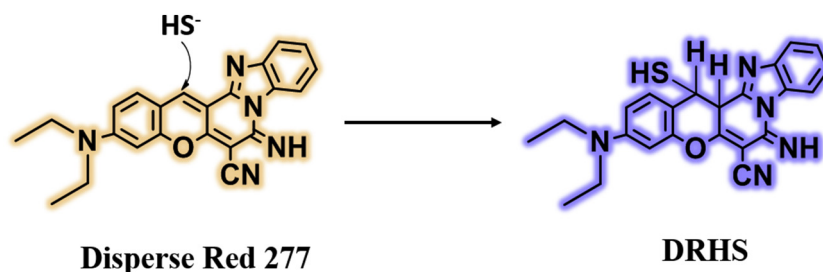


Fig. 6. Fluorescence spectral changes of **Disperse Red 277** (5.0 μ M in DMSO/HEPES buffer = 6/4) after incubation with different concentrations of **Na₂S** (0 \rightarrow 150 equiv.). Each spectrum was recorded after 60 s. The inset denotes the fluorescent change of **Disperse Red 277** (5.0 μ M) in the absence of **Na₂S** (left) and the presence of 150 equiv. **Na₂S** (right).

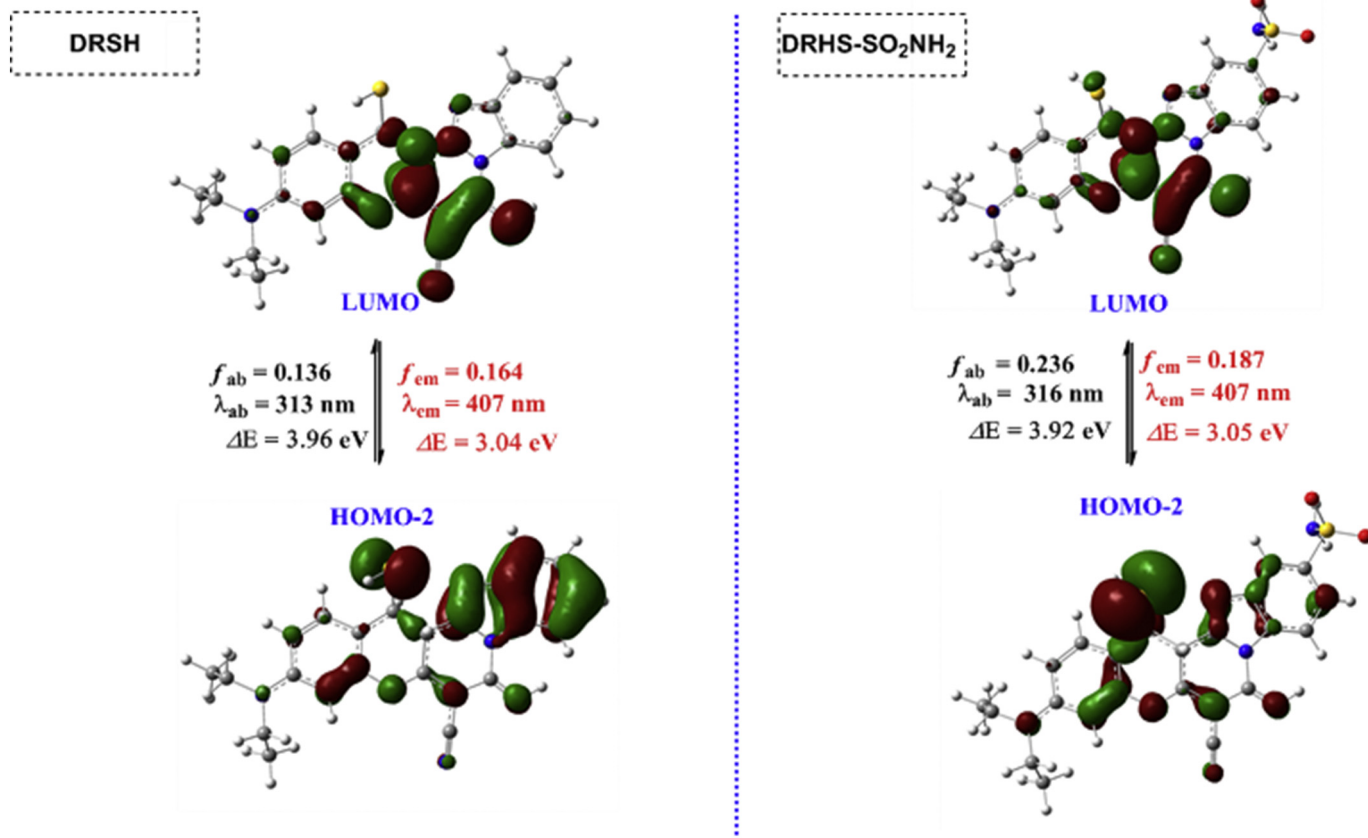
Scheme 2. Reaction mechanism for **Disperse Red 277** and HS^- .

3.4. Reaction mechanism

To further confirm our hypothesis and investigate the real detection mechanism, the following experiments are performed. First, the absorption and emission changes of **Disperse Red 277** upon the addition of different concentrations of Na_2S were measured to verify whether the fluorophore **Disperse Red 277** played any role in the detection of H_2S by the **DR-SO₂N₃** probe. It was observed that the absorptions at 329 and 555 nm apparently decreased while a new absorption peak appeared at approximately 374 nm (Fig. 5). This was accompanied by a color change from pink to almost colorless (inset of Fig. 5). Accordingly, the emission wavelength completely disappeared at 586 nm, whereas the intensity of the wavelength slightly increased at 418 nm upon excitation at 380 nm (Fig. 6). All the aforementioned results indicate that a new compound **DRHS** can be produced after the addition of HS^- to the **Disperse Red 277** solution. To our surprise, no fluorescence enhancement was observed in the fluorescent spectra at 586 nm when the

concentration of Na_2S became 5.0 μM (1 equiv.). Furthermore, the ratiometric response of the fluorescence intensities at 418 and 586 nm ($F_{418 \text{ nm}}/F_{586 \text{ nm}}$) increased from 0.054 to 0.27, with a final 5-fold enhancement factor. This indicates that the sulfonyl azide group of **DR-SO₂N₃** and the basic fluorophore **Disperse Red 277** play important roles in the highly selective and sensitive detection of H_2S . The spectral studies indicated that the sensing response of **Disperse Red 277** to Na_2S was most probably because of the formation of a new **DRHS** compound. Further, the possible response mechanism for the formation of **DRHS** is depicted in Scheme 2.

Because the isolation of the proposed final products **DRHS-SO₂NH₂** and **DRHS** failed, further evidence is required to corroborate their formation. Thus, mass spectrometry analysis of the products was performed after the reaction between **DR-SO₂N₃**, **Disperse Red 277**, and Na_2S . As depicted in Figs. S3 and S4, the peaks of the key products **DRHS-SO₂NH₂** ($m/z = 493.1$) and **DRHS** ($m/z = 414.1$) were observed in the reaction mixture, which is in accordance

Fig. 7. Frontier molecular orbitals of **DRHS** and **DRHS-SO₂NH₂**.

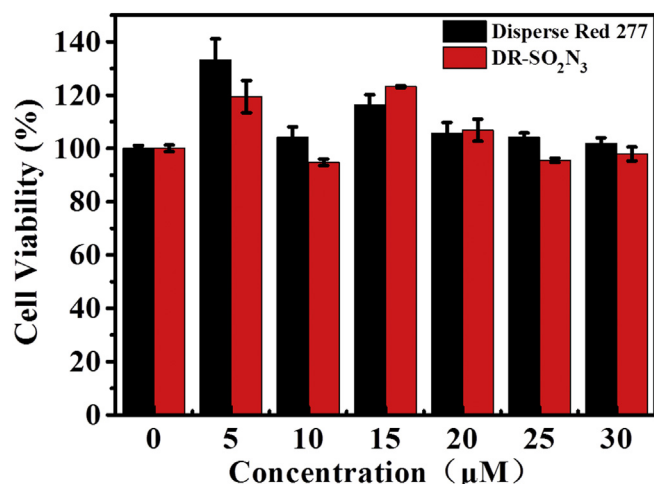


Fig. 8. MTT assay using the formazan absorbance at 570 nm for the biological toxicity of the MCF-7 cells in the presence of DR-SO₂N₃ and Disperse Red 277 after different incubation times. The mean values and standard deviations were obtained from three independent experimental determinations.

with our hypothesis and the results of the absorption and emission spectroscopy.

According to the aforementioned experiment and the proposed mechanism, when different concentrations of Na₂S were added to DR-SO₂N₃ and Disperse Red 277, the DRHS-SO₂NH₂ and DRHS compounds were obtained, and the relative long-wavelength absorption and emission bands disappeared. To clarify this phenomenon, we also performed DFT/TDDFT studies on DRHS-SO₂NH₂ and DRHS with the B3LYP/6-311 + G** method. The computational results denoted that no strong absorption peak was observed to be higher than 400 nm, which was consistent with the experimental observations. As depicted in Fig. 7, the relatively long absorption peak at 375 nm can be attributed to the HOMO-2 → LUMO transition (DRHS: $f_{ab} = 0.136$ and $\lambda_{ab} = 313$ nm; DRHS-SO₂NH₂: $f_{ab} = 0.236$ and $\lambda_{ab} = 316$ nm) (Table S5). In case of the frontier molecular orbitals, the HOMO-2 of DRHS was mainly occupied by the lone-pair electrons of the S atom and the π electrons of the benzimidazole moiety, while the LUMO was mainly located

on the coumarin and represented the π^* orbital. Thus, both the $n \rightarrow \pi^*$ and $\pi \rightarrow \pi^*$ transitions generated the absorption peak observed in the experiment. Further, the LUMO → HOMO-2 ($f_{em} = 0.164$ and $\lambda_{em} = 407$ nm) transition of DRHS was responsible for the emission peak of 418 nm in the experiment (Table S6). The calculated spectroscopic data for DRHS-SO₂NH₂ revealed almost similar electronic transitions to those of DRHS (Table S7), except for the HOMO-2 of DRHS-SO₂NH₂, which was mainly located on the S atom, and the absorption peak was mainly ascribed to the $n \rightarrow \pi^*$ transition. The LUMO → HOMO-2 transition ($f_{em} = 0.187$ and $\lambda_{em} = 407$ nm) contributed to the emission at 435 nm for DRHS-SO₂NH₂ (Table S8). Thus, the theoretical calculation is also in good agreement with the experimental mass spectra and our proposed mechanism.

3.5. The applications of probe DR-SO₂N₃

To evaluate the biological applicability of DR-SO₂N₃ and verify its permeability and cytotoxicity, the effect of DR-SO₂N₃ on cell proliferation was determined using the MTT assay in the living MCF-7 cell lines according to the reported literature. The accumulation behavior of DR-SO₂N₃ was assessed, and the viability of the cells was observed (Fig. 8). Meanwhile, the cytotoxicity for Disperse Red 277 was also investigated using the living MCF-7 cells. The DR-SO₂N₃ probe and Disperse Red 277 showed good permeability and no cytotoxicity to living cells in 0–30 μM (Fig. 8), which confirmed the applicability of the DR-SO₂N₃ probe and Disperse Red 277 for endogenous H₂S imaging.

Next, the ability of DR-SO₂N₃ for detecting the changes in exogenous H₂S in living cells was examined using confocal microscopy. The MCF-7 cells generated fluorescence in both the blue and red channels upon incubation using DR-SO₂N₃ (10 μM) for 0.5 h at 37 °C (Fig. 9). The cells were further treated with fresh medium containing Na₂S (150 μM) for an additional 15 min. We observed that in the presence of Na₂S, the luminescence intensity (blue channel) of the MCF-7 cells increased, whereas the fluorescence intensity (red channel) of the MCF-7 cells decreased (Fig. 9). As can be observed from Fig. 9, the I_{blue}/I_{red} ratio increased upon the exogenous addition of H₂S, which indicated that the DR-SO₂N₃ probe could quantitatively and ratiometrically detect the exogenous H₂S in living cells. Meanwhile, we also investigated whether Disperse Red 277 can realize the ratiometric detection of H₂S in living cells. As depicted in Fig. S4, the fluorescence intensity of the

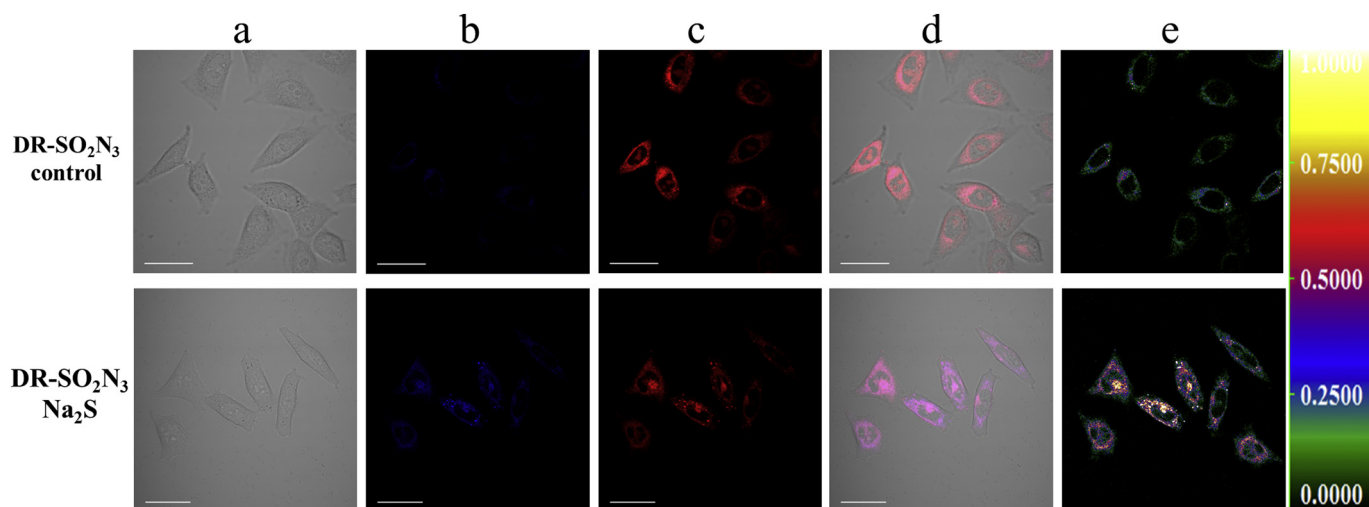


Fig. 9. Confocal fluorescence images of MCF-7 stained with DR-SO₂N₃ (10 μM) for 0.5 h before and after incubation with Na₂S (150 μM) for 15 min. (a) Bright images of the cells; (b) fluorescence images of the blue channels collected at 415–460 nm; (c) fluorescence images of the red channels collected at 575–620 nm; (d) overlap of the fluorescence and bright images; (e) ratiometric images of I_{blue}/I_{red} ; excitation wavelength at 405 nm. (For interpretation of the references to color in this figure legend, the reader is referred to the web version of this article.)

red channel exhibited a decrease after incubation with Na₂S (150 μM) for 15 min, whereas no enhancement was observed in that of the blue channel. A possible reason for this result is that the increase in the fluorescence intensity at the short wavelength of **Disperse Red 277** caused by H₂S is lower than that caused by DR-SO₂N₃ (Fig. 6), which makes it difficult to observe the enhancement of the blue channel fluorescence in cells. These results indicate that **Disperse Red 277** is not suitable for the ratiometric detection of endogenous H₂S in living cells.

4. Conclusion

In summary, we have rationally designed and synthesized a new fluorescent probe DR-SO₂N₃ at two reaction sites. The rapid reduction and nucleophilic addition of H₂S resulted in the high selectivity and sensitivity of DR-SO₂N₃ for H₂S in vitro. The DR-SO₂N₃ probe reached a detection limit of 2.46 μM and exhibited a rapid ratiometric fluorescence response to H₂S with a final 619-fold enhancement factor (F_{435 nm}/F_{584 nm}). These properties render the DR-SO₂N₃ probe suitable for the ratiometric monitoring of H₂S in vivo. Further, the photophysical properties of this probe and the final reaction product were investigated using the DFT/TDDFT calculation and verified the correction of our proposed mechanism. We believe that this probe may be useful to explore the function of H₂S in biological systems in the future.

Acknowledgements

This work was supported by the NSF of China (21606032, 21704011 and 21706021, scientific research general project No. L2015053 from Liaoning Provincial Education Department, the doctoral scientific research foundation No. 201501192 of Liaoning province, the State Key Laboratory of Fine Chemicals (KF 1608 and KF1713), and Dalian science and technology innovation fund (2018J12GX056), Dalian youth science and technology star fund (2018RQ46).

Appendix A. Supplementary data

Supplementary data to this article can be found online at <https://doi.org/10.1016/j.saa.2019.117391>.

References

- H. Li, W. Peng, W. Feng, Y. Wang, G. Chen, S. Wang, et al., A novel dual-emission fluorescent probe for the simultaneous detection of H₂S and GSH, *Chem. Commun.* 52 (25) (2016) 4628–4631.
- S. Ding, G. Feng, Smart probe for rapid and simultaneous detection and discrimination of hydrogen sulfide, cysteine/homocysteine, and glutathione, *Sensor. Actuat. B-chem.* 235 (2016) 691–697.
- W. Wang, C. Wu, C. Yang, G. Li, Q.-B. Han, S. Li, et al., A dual-functional luminescent probe for imaging H₂S in living zebrafish and discrimination hypoxic cells from normoxic cells, *Sensor. Actuat. B-chem.* 255 (2018) 1953–1959.
- F. Gallyas, Involvement of redox-signalling in endogenous hydrogen sulfide production, *Br. J. Pharmacol.* 166 (8) (2012) 2228–2230.
- Y. Zhao, Matthew M. Cerda, M.D. Pluth, Fluorogenic hydrogen sulfide (H₂S) donors based on sulfenyl thiocarbonates enable H₂S tracking and quantification, *Chem. Sci.* 10 (2019) 1873–1878.
- J. Liu, X. Chen, Y. Zhang, G. Gao, X. Zhang, S. Hou, et al., A novel 3-hydroxychromone fluorescent probe for hydrogen sulfide based on an excited-state intramolecular proton transfer mechanism, *New J. Chem.* 42 (15) (2018) 12918–12923.
- J.T. Hancock, M. Whiteman, Hydrogen sulfide and cell signaling: team player or referee? *Plant Physiol. Biochem.* 78 (2014) 37–42.
- D. Qiao, T. Shen, M. Zhu, X. Liang, L. Zhang, Z. Yin, et al., A highly selective and sensitive fluorescent probe for simultaneously distinguishing and sequentially detecting H₂S and various thiol species in solution and in live cells, *Chem. Commun.* 54 (2018) 13252–13255.
- D. Chao, X. He, Y. Yang, G. Balboni, S. Salvadori, D.H. Kim, et al., Hydrogen sulfide induced disruption of Na⁺ homeostasis in the cortex, *Toxicol. Sci.* 128 (1) (2012) 198–208.
- P. Kamoun, M.-C. Belardinelli, A. Chabli, K. Lallouchi, B. Chadeaux-Vekemans, Endogenous hydrogen sulfide overproduction in down syndrome, *Am. J. Med. Genet. A* 116A (3) (2003) 310–311.
- S. Fiorucci, E. Antonelli, A. Mencarelli, S. Orlandi, B. Renga, G. Rizzo, et al., The third gas: H₂S regulates perfusion pressure in both the isolated and perfused normal rat liver and in cirrhosis, *Hepatology* 42 (3) (2005) 539–548.
- H. Peng, Y. Cheng, C. Dai, A.L. King, B.L. Predmore, D.J. Lefer, et al., A fluorescent probe for fast and quantitative detection of hydrogen sulfide in blood, *Angew. Chem. Int. Ed. Engl.* 50 (41) (2011) 9672–9675.
- M.N. Hughes, M.N. Centelles, K.P. Moore, Making and working with hydrogen sulfide: the chemistry and generation of hydrogen sulfide in vitro and its measurement in vivo: a review, *Free Radic. Biol. Med.* 47 (10) (2009) 1346–1353.
- D. Jiménez, R. Martínez-Máñez, F. Sancenón, J.V. Ros-Lis, A. Benito, J. Soto, A new chromo-chemodosimeter selective for sulfide anion, *J. Am. Chem. Soc.* 125 (30) (2003) 9000–9001.
- B. Gurrám, S. Zhang, M. Li, H. Li, Y. Xie, H. Cui, et al., Celecoxib conjugated fluorescent probe for identification and discrimination of Cyclooxygenase-2 enzyme in Cancer cells, *Anal. Chem.* 90 (8) (2018) 5187–5193.
- H. Li, J. Fan, S. Long, J. Du, J. Wang, X. Peng, A fluorescent and colorimetric probe for imaging the mitochondrial sulfur dioxide in living cells, *Sensor. Actuat. B-chem.* 273 (2018) 899–905.
- H. Li, Q. Yao, F. Xu, N. Xu, R. Duan, S. Long, et al., Imaging gamma-Glutamyltranspeptidase for tumor identification and resection guidance via enzyme-triggered fluorescent probe, *Biomaterials* 179 (2018) 1–14.
- H. Li, Q. Yao, F. Xu, N. Xu, X. Ma, J. Fan, et al., Recognition of exogenous and endogenous Nitroxyl in living cells via a two-photon fluorescent probe, *Anal. Chem.* 90 (7) (2018) 4641–4648.
- J. Du, Q. Gu, J. Chen, J. Fan, X. Peng, A novel fluorescent probe for the ratiometric recognition of protein based on intramolecular charge transfer, *Sensor. Actuat. B-chem.* 265 (2018) 204–210.
- J. Du, T. Zhu, Q. Gu, W. Cao, J. Fan, X. Peng, Fabrication of artificial fluorescent protein probe for HSA recognition and relay sensing Ag⁺ by functional microenvironment-sensitive fluorescent dye, *Sensor. Actuat. B-chem.* 263 (2018) 661–667.
- C. Liu, F. Wang, T. Xiao, B. Chi, Y. Wu, D. Zhu, et al., The ESIPF fluorescent probes for N₂H₄ based on benzothiazol and their applications for gas sensing and bioimaging, *Sensor. Actuat. B-chem.* 256 (2018) 55–62.
- K. Sasakura, K. Hanaoka, N. Shibuya, Y. Mikami, Y. Kimura, T. Komatsu, et al., Development of a highly selective fluorescence probe for hydrogen sulfide, *J. Am. Chem. Soc.* 133 (45) (2011) 18003–18005.
- X. Jiao, Y. Xiao, Y. Li, M. Liang, X. Xie, X. Wang, et al., Evaluating drug-induced liver injury and its remission via discrimination and imaging of HClO and H₂S with a two-photon fluorescent probe, *Anal. Chem.* 90 (12) (2018) 7510–7516.
- K. Liu, C. Liu, H. Shang, M. Ren, W. Lin, A novel red light emissive two-photon fluorescent probe for hydrogen sulfide (H₂S) in nucleolus region and its application for H₂S detection in zebrafish and live mice, *Sensor. Actuat. B-chem.* 256 (2018) 342–350.
- K. Rajalakshmi, Y.-S. Nam, S. Youg, M. Selvaraj, K.-B. Lee, Biocompatible silica nanoparticles conjugated with azidocoumarin for trace level detection and visualization of endogenous H₂S in PC3 cells, *Sensor. Actuat. B-chem.* 259 (2018) 307–315.
- B. Zhao, Y. Yang, Y. Wu, B. Yang, J. Chai, X. Hu, et al., To re-evaluate the emission mechanism, AIE activity of 5-azidofluorescein and its reaction with H₂S and NO, *Sensor. Actuat. B-chem.* 256 (2018) 79–88.
- B. Ke, W. Wu, W. Liu, H. Liang, D. Gong, X. Hu, et al., Bioluminescence probe for detecting hydrogen sulfide in vivo, *Anal. Chem.* 88 (1) (2016) 592–595.
- Z. Wu, Z. Li, L. Yang, J. Han, S. Han, Fluorogenic detection of hydrogen sulfide via reductive unmasking of o-azidomethylbenzoyl-coumarin conjugate, *Chem. Commun.* 48 (81) (2012) 10120–10122.
- S.K. Das, C.S. Lim, S.Y. Yang, J.H. Han, B.R. Cho, A small molecule two-photon probe for hydrogen sulfide in live tissues, *Chem. Commun.* 48 (67) (2012) 8395–8397.
- G.J. Mao, T.T. Wei, X.X. Wang, S.Y. Huan, D.Q. Lu, J. Zhang, et al., High-sensitivity naphthalene-based two-photon fluorescent probe suitable for direct bioimaging of H₂S in living cells, *Anal. Chem.* 85 (16) (2013) 7875–7881.
- H. Zhang, Y. Xie, P. Wang, G. Chen, R. Liu, Y.W. Lam, et al., An iminocoumarin benzothiazole-based fluorescent probe for imaging hydrogen sulfide in living cells, *Talanta* 135 (2015) 149–154.
- H. Zhang, P. Wang, G. Chen, H.Y. Cheung, H. Sun, A highly sensitive fluorescent probe for imaging hydrogen sulfide in living cells, *Tetrahedron Lett.* 54 (36) (2013) 4826–4829.
- G. Zhou, H. Wang, Y. Ma, X. Chen, An NBD fluorophore-based colorimetric and fluorescent chemosensor for hydrogen sulfide and its application for bioimaging, *Tetrahedron* 69 (2) (2013) 867–870.
- J. Kang, F. Huo, C. Yin, A novel ratiometric fluorescent H₂S probe based on tandem nucleophilic substitution/cyclization reaction and its bioimaging, *Dyes Pigments* 146 (2017) 287–292.
- J. Men, X. Yang, H. Zhang, J. Zhou, A near-infrared fluorescent probe based on nucleophilic substitution–cyclization for selective detection of hydrogen sulfide and bioimaging, *Dyes Pigments* 153 (2018) 206–212.
- J. Lv, F. Wang, J. Qiang, X. Ren, Y. Chen, Z. Zhang, X. Chen, Enhanced response speed and selectivity of fluorescein-based H₂S probe via the cleavage of nitrobenzene sulfonfyl ester assisted by ortho aldehyde groups, *Biosens. Bioelectron.* 87 (2017) 96–100.
- Y. Ji, L.J. Xia, L. Chen, X.F. Guo, H. Wang, H.J. Zhang, A novel BODIPY-based fluorescent probe for selective detection of hydrogen sulfide in living cells and tissues, *Talanta* 181 (2018) 104–111.
- W. Sun, J. Fan, C. Hu, J. Cao, H. Zhang, X. Xiong, et al., A two-photon fluorescent probe with near-infrared emission for hydrogen sulfide imaging in biosystems, *Chem. Commun.* 49 (37) (2013) 3890–3892.
- X.L. Liu, X.J. Du, C.G. Dai, Q.H. Song, Ratiometric two-photon fluorescent probes for mitochondrial hydrogen sulfide in living cells, *J. Org. Chem.* 79 (20) (2014) 9481–9489.
- J. Zhang, R. Wang, Z. Zhu, L. Yi, Z. Xi, A FRET-based ratiometric fluorescent probe for visualizing H₂S in lysosomes, *Tetrahedron* 71 (45) (2015) 8572–8576.

- [41] G. Yang, J. Zhang, S. Zhu, Y. Wang, X. Feng, M. Yan, et al., Fast response and highly selective detection of hydrogen sulfide with a ratiometric two-photon fluorescent probe and its application for bioimaging, *Sensor. Actuat. B-chem.* 261 (2018) 51–57.
- [42] L. He, X. Yang, K. Xu, X. Kong, W. Lin, A multi-signal fluorescent probe for simultaneously distinguishing and sequentially sensing cysteine/homocysteine, glutathione, and hydrogen sulfide in living cells, *Chem. Sci.* 8 (9) (2017) 6257–6265.
- [43] S.J. Li, Y.F. Li, H.W. Liu, D.Y. Zhou, W.L. Jiang, J. Ou-Yang, et al., A dual-response fluorescent probe for the detection of viscosity and H₂S and its application in studying their cross-talk influence in mitochondria, *Anal. Chem.* 90 (15) (2018) 9418–9425.
- [44] H.S. Jung, K.C. Ko, G.H. Kim, A.R. Lee, Y.C. Na, C. Kang, et al., Coumarin-based thiol Chemosensor: synthesis, Turn-on mechanism, and its biological application, *Org. Lett.* 13 (6) (2011) 1498–1501.
- [45] J.C. Raboin, M. Beley, G. Kirsch, Pyridine-fused coumarins: a new class of ligands for ruthenium complexes with enhanced spectral absorption, *Tetrahedron Lett.* 41 (8) (2000) 1175–1177.
- [46] W. Li, W. Sun, X. Yu, L. Du, M. Li, Coumarin-based fluorescent probes for H₂S detection, *J. Fluoresc.* 23 (1) (2013) 181–186.
- [47] S.T. Huang, J.L. Jian, H.Z. Peng, K.L. Wang, C.M. Lin, C.H. Huang, et al., The synthesis and optical characterization of novel iminocoumarin derivatives, *Dyes Pigments* 86 (1) (2010) 6–14.
- [48] E. Roussakis, S. Voutsadaki, E. Pinakoulaki, D.P. Sideris, K. Tokatlidis, H.E. Katerinopoulos, ICPBCZin: a red emitting ratiometric fluorescent indicator with nanomolar affinity for Zn²⁺ ions, *Cell Calcium* 44 (3) (2008) 270–275.
- [49] J. Liu, Y.Q. Sun, J. Zhang, T. Yang, J. Cao, L. Zhang, et al., A ratiometric fluorescent probe for biological signaling molecule H₂S: fast response and high selectivity, *Chem. Eur. J.* 19 (15) (2013) 4717–4722.
- [50] L. Jiao, F. Song, J. Cui, X. Peng, A near-infrared heptamethine aminocyanine dye with a long-lived excited triplet state for photodynamic therapy, *Chem. Commun.* 54 (66) (2018) 9198–9201.